



SEISMIC VULNERABILITY OF MOTORWAY BRIDGE ON ACTIVE LANDSLIDE

M. Loli⁽¹⁾, A. Chatzidaki⁽²⁾, D. Vamvatsikos⁽³⁾, G. Gazetas⁽⁴⁾

⁽¹⁾ Postdoctoral researcher, National Technical University of Athens, mariannaloli@yahoo.com

⁽²⁾ PhD candidate, National Technical University of Athens, cakrivi@central.ntua.gr

⁽³⁾ Assistant Professor, National Technical University of Athens, divamva@central.ntua.gr

⁽⁴⁾ Emeritus Professor, National Technical University of Athens, gazetas@central.ntua.gr

Abstract

The western section of Egnatia Odos motorway in Greece runs through a challenging mountainous terrain where geohazards are exacerbated by moderate seismicity. Located a few kilometers east of the town of Metsovo, the twin girder bridges of the Panagia interchange have their central piers founded on an active landslide. Being part of a research project that aims to develop a tool for rapid inspection and assessment of the motorway, this study presents a thorough seismic vulnerability analysis of the hybrid caisson–pile group foundation system that supports the most critical piers of the interchange. This foundation system has been designated as a slope stabilizing measure, in addition to carrying the loads transmitted by the bridge superstructure. Numerical modelling with nonlinear 3D finite elements has been employed, together with site-specific hazard-consistent selection of ground motion records. A hybrid numerical approach has been developed using segregated models of varying refinement with rational approximation of interactions between the nonlinear response of soil, the movement of the slope, the kinematic distress imposed upon the foundation and the inertial loads from the vibration of the superstructure. The method estimates pile performance under large-scale, dynamic landslide action with sufficient engineering accuracy for cases where slope actions dominate the response. The softening behavior of the sliding surface is calibrated versus monitored slope displacements. The effect of groundwater recharge after heavy rainfall is incorporated in the vulnerability analysis in a simplified manner, using different scenarios for water table elevation. Focusing on the performance of the foundations, damage is described in terms of their permanent displacements and curvatures. Results indicate that a range of excitations with an exceedance probability of 2% in 50 years are capable of inflicting substantial permanent pile damage, even complete failure, if combined with a fully saturated soil condition. The computed residual foundation displacements can serve as input for a detailed structural model simulating the performance of the superstructure for estimating the bridge vulnerability.

Keywords: seismic hazard, landslides, numerical modelling, soil – structure interaction, vulnerability analysis



1. Introduction

The Panagia Interchange of Egnatia Odos (motorway) in Greece is a typical T-girder beam bridge (Fig. 1). It consists of two twin branches with an average span of approximately 37 m and considerable pier height, reaching up to 25 m. It is a modern structure with decks supported on elastometallic anchored rubber bearings. Part of the bridge is founded on a precarious slope (Fig. 2a) and is prone to significant permanent displacements as a result of seismic activity in addition to rainfall.

A preliminary monitoring campaign was launched before construction of the bridge, in 2007, involving mainly the installation of inclinometers in the area. As shown in Fig. 2a, significant displacements have been recorded, especially in locations NIN1 and NIN2. Analysis of inclinometer readings has led to the identification of a landslide area that interacts with the foundations of the central piers only, namely P4, P5, and P6 according to Fig. 2b. Owing to its topography (especially slope inclination), the cross-section pictured in Fig. 2c, in the vicinity of P5, has been recognized as the most critical. Here, the unstable soil layer is relatively shallow, ranging in depth from 8.5 m to 10.5 m, and the measured distributions of horizontal displacements with depth, as per Fig. 2d, indicate strain accumulation upon a thin zone of soil (slip plane).



Fig. 1 – Photos of the Panagia Interchange (PI) located 17 km northeast of Metsovo, Greece.

The stability of P5(L) and P5(R) is largely dependent on their massive foundations, which by design were intended to act also as a slope stabilizing measure. The foundations consist of a 32 m deep, reinforced concrete, circular caisson with a diameter of 7 m. Its capacity is strengthened by a total of 20 Φ 80 piles installed in its perimeter. The piles are isolated from the caisson mass and are only indirectly connected to it through the rigid cap, as discussed in the following. The design has accounted for seismic actions, as the region is prone to moderate seismicity.

The site has been studied in the framework of the PANOPTIS EU funded research project aiming to develop a multi-hazard risk and resilience assessment platform for efficient management of the motorway. This paper presents results from a thorough analytical study of the bridge which was carried out for the purpose of developing case-specific fragility curves. A component-based, hybrid approach has been engaged to this end, employing segregated models of varying refinement with rational approximation of interactions between the nonlinear response of soil, the movement of the slope, the kinematic distress imposed upon the foundation and the inertial loads from the vibration of the superstructure. Due to space limitations, this paper focuses on the response of the foundation to the most detrimental of the considered hazard scenarios: intense seismic excitation (consistent with the seismic hazard at a probability of exceedance of 2% in 50 years) with the water table at its highest possible level.

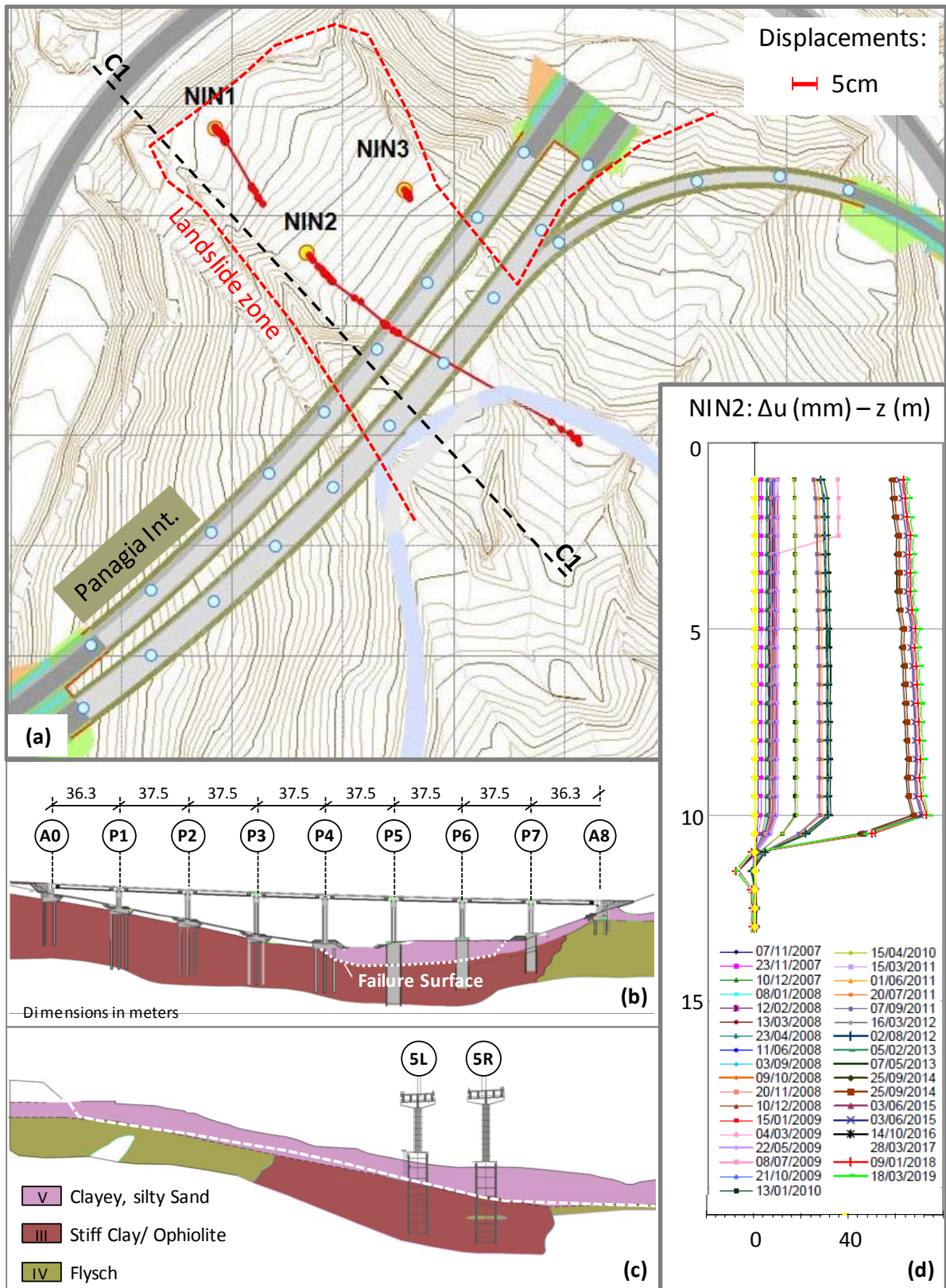


Fig. 2 – Interaction with an active landslide: (a) topographic map indicating location of inclinometers; (b) longitudinal cross-section of the left branch of the bridge; (c) geometry of the most critical cross-section C1; and (d) distribution of horizontal displacements recorded at NIN2 from 07/11/2007 to 18/03/2019.

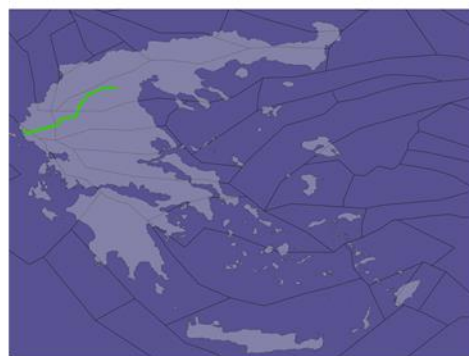


2. Definition of the Seismic Hazard

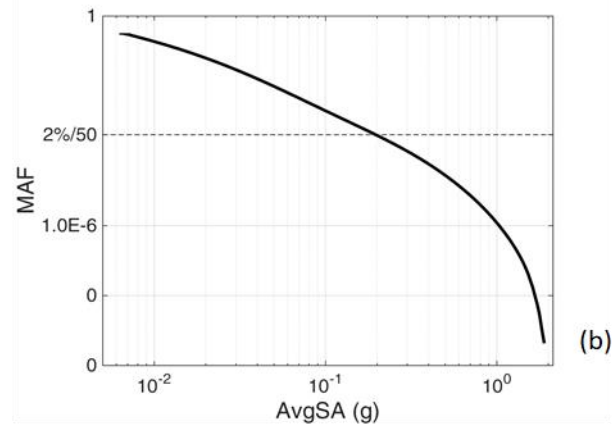
The OpenQuake opensource software [1] is used for performing the seismic hazard and disaggregation analyses, by employing the area source model of the SHARE project [2] (Fig. 3a) and the ground motion prediction equation proposed by Boore and Atkinson [3]. The state-of-the-art average spectral acceleration, $AvgSa$, ([4]-[6]) is adopted as the Intensity Measure (IM):

$$AvgSa(T_{Ri}) = \left(\prod_{i=1}^n Sa(T_{Ri}) \right)^{1/n} \quad (1)$$

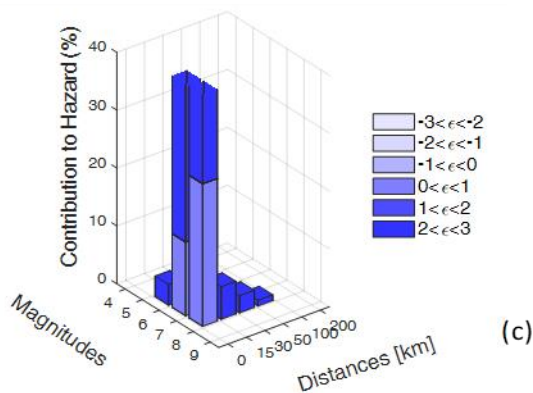
It is estimated by combining n spectral acceleration ordinates, Sa , at periods T_{Ri} . Each ordinate is the geometric mean of the 5%-damped spectral acceleration from the two horizontal components. Herein, the period range of [0.3 sec, 3.0 sec] with an increment of 0.1 sec is adopted. The site-specific seismic hazard curve is presented in Fig. 3b in terms of $AvgSa$ and the mean annual frequency (MAF) of exceeding it. Disaggregation analysis is performed for the seismic hazard corresponding to an exceedance probability of 2% in 50 years, or equivalently a MAF of $-\ln(1-0.02)/50=0.000404$, to determine how each magnitude, distance and epsilon (ϵ) combination contributes to the seismic hazard (Fig. 3c). The mean disaggregation scenario is used to determine the Conditional Spectrum ([7, 8]) for selecting a set of 11 ground motion records that are consistent with the site hazard. The conditional mean spectrum, its 2.5th and 97.5th percentiles (CMS $\pm 2\sigma$) and the response spectra of the selected records are presented in Fig. 3d.



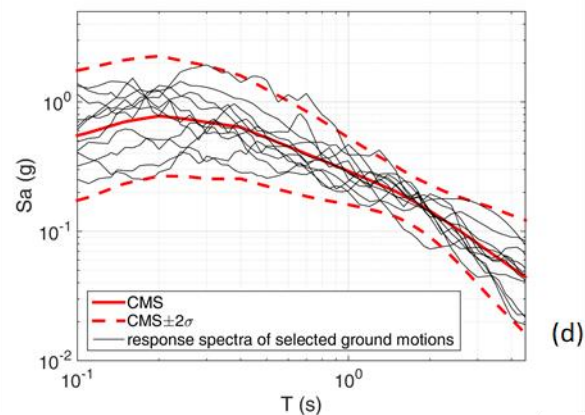
(a)



(b)



(c)



(d)

Fig. 3 – Seismic hazard assessment and CS-based record selection: (a) SHARE area source model for Greece and the Egnatia Odos segment (green line); (b) site-specific seismic hazard curve; (c) disaggregation analysis results for the 2% in 50 years hazard level; (d) CMS, CMS $\pm 2\sigma$ and response spectra of the 11 selected ground motion records.



3. FE Modelling

3.1 Numerical method

Slope stability analysis by elastoplastic Finite Elements (FE) can be accurate, robust and simple enough for routine use by practicing engineers, eg. [9-10]. Nonlinear analyses were carried out in the ABAQUS FE package to study the response of pier 5L (Fig. 2c), which was judged as the most vulnerable due to its location with respect to the slope. Its foundation was assumed isolated from the neighboring structures (of both bridge branches), as the pier-to-pier distance is large enough to neglect interaction (distance > 3 times the caisson diameter). Use of three-dimensional FE modelling is necessary to tackle important soil–foundation interaction effects, taking account of the exact geometry, kinematic boundaries, and pile group response. The need to sufficiently discretize piles did not allow simulation of their geometry within the environment of the entire landslide. Such a model would require millions of elements rendering time-history analysis practically impossible. However, pile response is of critical importance for the assessment of the system performance. An alternative, hybrid approach was adopted, involving two different (in size and refinement) models, as well as two different computational steps. Specifically:

Step 1: Analysis of the dynamic interaction between the slope and the pier–foundation system using model A (Fig. 4). This model simulates a total plan area of 290 m x 37 m of the slope. At this scale, pile geometry is ignored and the hybrid foundation is reduced to a caisson with diameter equal to the total diameter of the assembly (equal to the diameter of the cap that connects them). Here, the additional resistance provided by the pile group is incorporated roughly by adding a beam of equivalent bending strength and stiffness in the middle of the caisson. The soil is modelled with nonlinear 8-nodal continuum elements while the pier column is modelled as a nonlinear beam with moment–curvature ($M-C_s$) relationship corresponding to the actual reinforced concrete section, as derived by section analysis. Particular care was taken for the simulation of the failing zone, highlighted in red color in Fig 4, as discussed in the following section. Interface behavior was taken into account, allowing sliding (with friction coefficient $\mu = 0.5$) and loss of contact between the foundation and the soil. The deck is assumed as a lumped mass and its continuity is accounted for through nonlinear horizontal and rotational springs. The latter were estimated according to relationships from the literature [11] assuming linear degradation of stiffness for deck displacements exceeding 10 cm. A dashpot was also added at the level of the deck to reproduce the damping effect of elastomeric bearings (assuming $\zeta = 2\%$). Appropriate free field boundaries were used at the sides of model A and dashpots were distributed at the base to absorb reflected seismic waves.

Step 2: Analysis of a refined model (model B), where the particular configuration of the foundation is reproduced precisely (Fig. 5a). Here, each pile is modeled as a 3D beam element circumscribed by 8-noded hexahedral solid elements (Fig. 5b). Every node of the beam is connected with the circumferential solid element nodes at the same height through appropriate kinematic constraints (implying that the pile remains undeformed in its cross-section). The pile stiffness and nonlinear section capacity ($M-C_s$) are introduced into the FE code as properties of the central beam, while the surrounding elements have zero rigidity and serve the sole purpose of capturing 3D effects. This step focuses on a representative region of soil around the pile, with dimensions $10D \times 5D$ (where D is the diameter of the pile cap), instead of modeling the whole slope-soil-foundation system (Fig. 5c). Symmetry along the foundation centerline was taken advantage of to allow simulation of half of the problem geometry. The resistance of the piles is computed by imposing a uniform displacement profile onto the boundary of the model (Fig. 5d), which is a reasonable approximation of landslide actions [12]. The depth of the dislocated horizontal soil layer is equal to the depth of the slip plane at the location of the foundation (10 m). Presumably, step 2 eliminates the effect of inertial actions on pile response. This is a simplification of reality, where damage is expected as a result of the combined action of kinematic-landslide loads and inertial loads. Nevertheless, results from preliminary un-coupled analyses indicated that the aseismic design of the pile group is quite conservative, leading to negligible pile damage when seismic actions are imposed separately. By contrast, the effect of kinematic loads is dominant, justifying our decision to evaluate pile damage based on results from step 2.

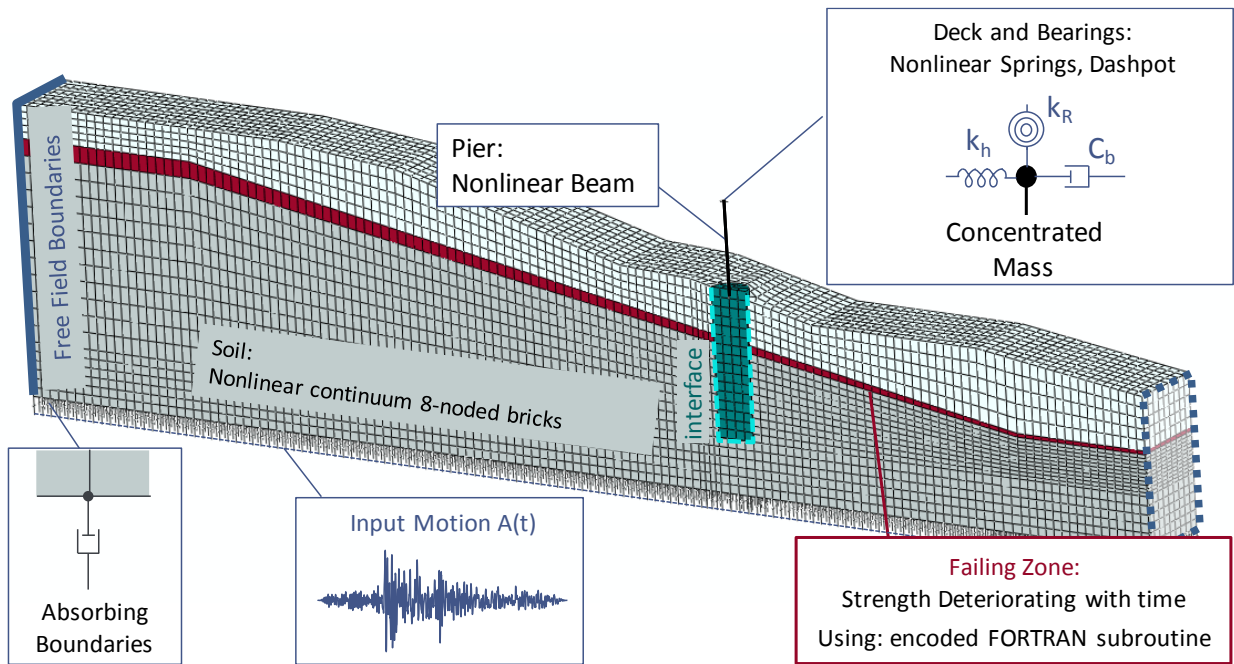


Fig. 4 – Details of model A and the numerical assumptions governing analytical Step 1.

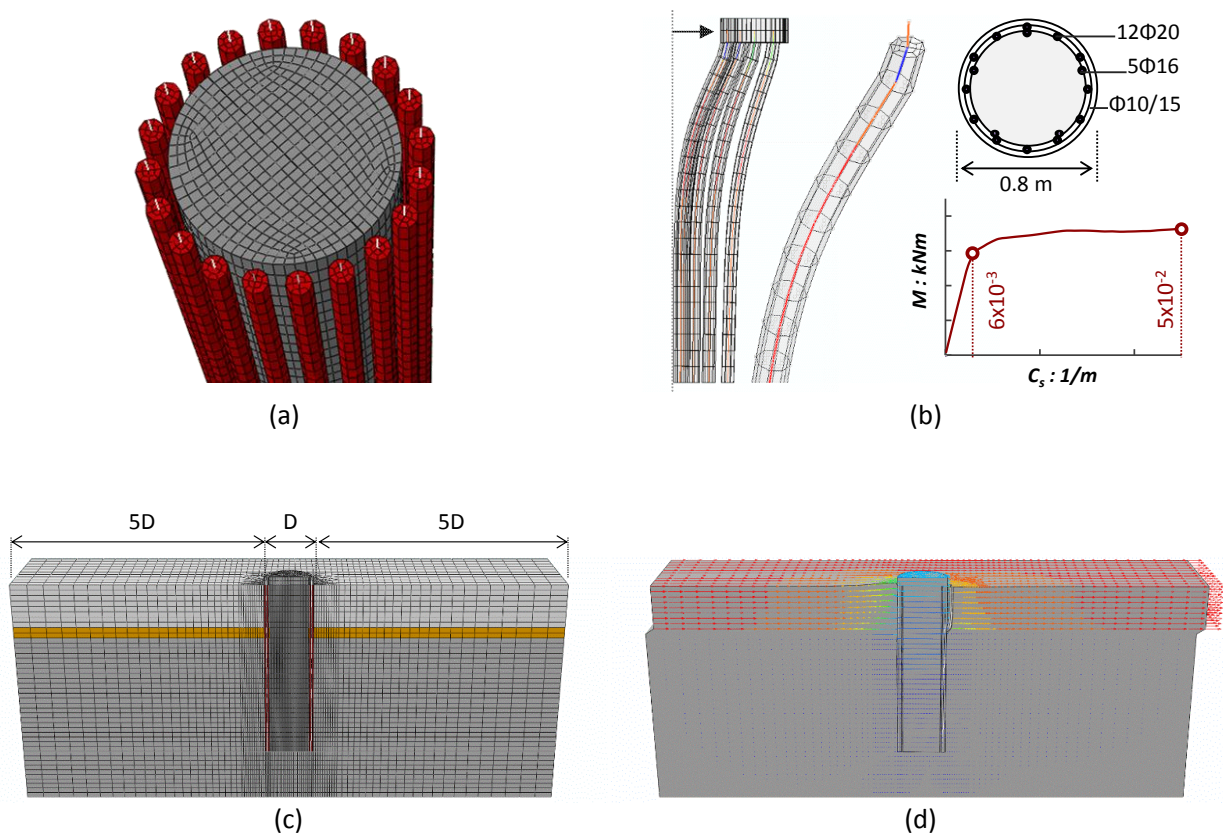


Fig. 5 – Details of the refined model used in Step 2: (a) configuration of the caisson – pile group assembly; (b) modelling of nonlinear pile response; (c) geometry of the refined model highlighting different soil materials; and (d) deformed mesh with superimposed vectors of horizontal displacements.



3.1 Constitutive modelling of soil

Constitutive modelling of the different soil materials was based on the results of a geotechnical survey (summarized in Table 1) and employed consistently in both analytical steps. Apart from the narrow zone of elements that simulates the slip plane, the different soil layers (namely III, IV, V according to the stratification shown in Fig 2c) were prescribed a kinematic hardening constitutive model incorporating the Von Mises plasticity failure criterion and associated flow rule. The model is appropriate for the description of the non-linear hysteretic behavior of cohesive materials and its capacity to simulate soil-structure interaction systems under seismic loading has been extensively validated in [13].

An elastoplastic constitutive model with Mohr-Coulomb failure criterion and isotropic strain softening was used for the soil in the failing zone. In this zone, pre-yield behavior is modeled as linear elastic with secant share modulus $G_s = t_y/\gamma_y$ equal to the G_s , as the latter has been derived from element tests (Soil V, according to table 1). Post-peak material softening [14] is accounted for through a reduction of the mobilized friction angle (ϕ) and dilation angle (ψ) with the increase of octahedral plastic strain. According to the model proposed by [15], we have assumed a linear decrease of ϕ and ψ , from peak (ϕ^{peak} , ψ^{peak}) to residual values (ϕ^{res} , ψ^{res}). The model was calibrated in order to macroscopically reproduce the deteriorating behavior that has led to the considerable slope displacements measured since 2007 (Fig. 6). The degradation of strength implied by the evolution of slope displacements shown in Fig. 6b is probably triggered by periods of excess rainfall that caused significant rise of the water table and thereby increased pore pressures. Yet, there is no record of the latter and the exact loading conditions are uncertain. The behavior of the slope from 2007 until today was therefore simulated as a period of gradual $c-\phi$ reduction. The relationship controlling degradation of strength with strain and time was calibrated with respect to measured displacements and encoded in the analysis through a user subroutine. A relatively satisfactory comparison was achieved, as shown in Fig. 6, assuming: $c = 5$ kPa, $\phi^{peak} = 33^\circ$, $\psi^{peak} = 3^\circ$ in 10/2007 and $c = 0$ kPa, $\phi^{res} = 18^\circ$, $\psi^{res} = 0^\circ$ in 08/2019.

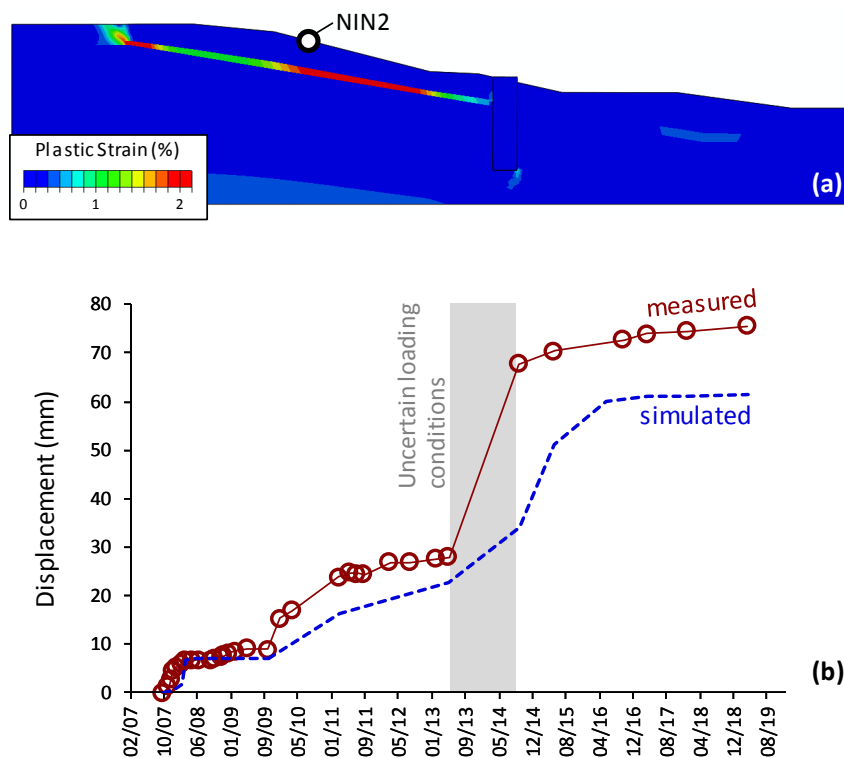


Fig. 6 – Calibration of weak zone material properties: (a) snapshot from $c-\phi$ reduction analysis highlighting accumulation of plastic strains; and (b) comparison between computed and measured displacements.



Table 1 – Measured geotechnical parameters.

	Zone	V	III	IV
SPT count number	N_{SPT}	16 (14-19)	43	16
1-D Compression Index	E_m [Mpa]	-	50	>900
Water content	w (%)	1.1	11.8	-
Specific weight	γ [kN/m ³]	21.6	24.2	25
Void ratio	e	0.439	-	0.439
Effective friction angle	ϕ' [deg]	33	24	35
Effective cohesion	c' [kPa]	5	35	70
Residual friction angle	ϕ'_r	18	20	-
Undrained shear strength	C_u [kPa]	70	220	-
Permeability	K [cm/s]	4.6×10^{-5}	2.4×10^{-5}	1×10^{-5}

4. Seismic Performance of the Foundation System

A scenario-based approach has been adopted as summarized in Table 2. Seismic motions that are consistent to three different levels of the seismic hazard were assumed to take place at the current (08/2019) strain-strength condition of the slope assuming two different, extreme scenarios for water table height: (i) low water table, i.e. the soil above the slip-plane is dry, and (ii) maximum water height, i.e. the entire moving mass of soil is fully saturated. In the latter case, the effect of pore pressures in reducing the effective stress and thereby the strength of the weak zone is indirectly taken into by proportionally reducing the effective friction angle (ϕ') in the calculations of the previously mentioned user subroutine. In the following, results are presented for only one of the investigated scenarios, which is in fact the most detrimental: intense earthquake (consistent with the seismic hazard at a probability of exceedance 2% in 50 years) taking place when the water table is at the maximum possible height, i.e. after an extended period of rainfall.

Table 2 – Summary of different hazard scenarios considered in the vulnerability study. Highlighted is the most detrimental one, where the focus of this paper is placed.

Water table Level:		Min.	Max.
Weak Earthquake	[20% in 50 years]	11 motions	11 motions
Moderate Earthquake	[10% in 50 years]	11 motions	11 motions
Strong Earthquake	[2% in 50 years]	11 motions	11 motions

Eleven different seismic motions have been used as excitation at the base of the FE model (Fig. 7). For this level of intensity, results from analytical Step 1 imply mobilization of the failure surface and significant slope movement (Fig. 8). Residual displacements of the slope with reference to location NIN2 (Fig. 8b), which is within the failure wedge, range from 0.5 m to over 3 m depending on the details of the excitation. It is interesting to observe that one specific excitation, namely HCMP-015, is far more detrimental than the others. This is attributable to the fact that this particular motion contains a large number of excitation cycles with considerable magnitude and highlights the significance of involving seismic motions of varying characteristics in such studies of slope vulnerability.

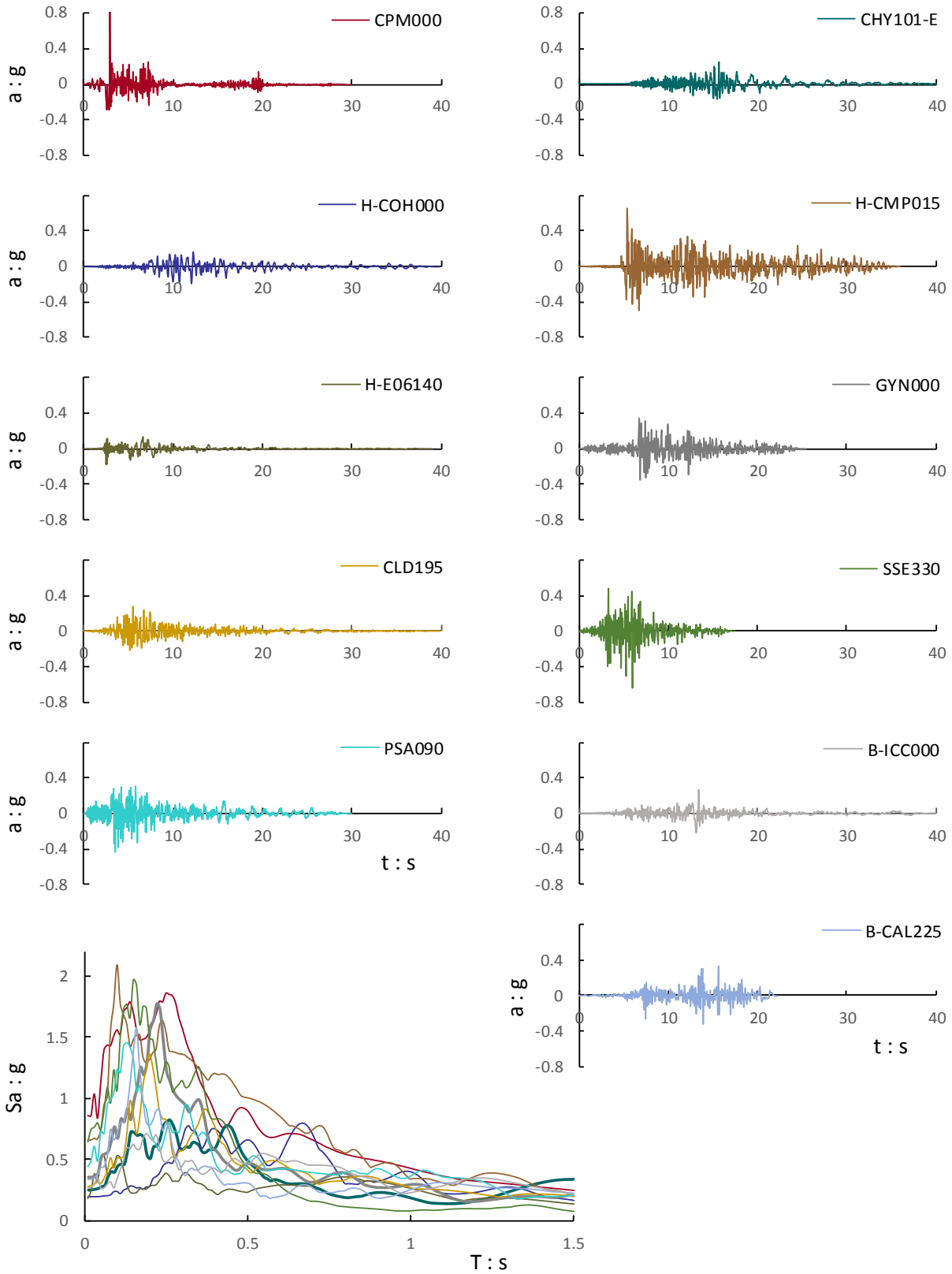


Fig. 7 – Acceleration time histories and elastic ($\xi = 5\%$) response spectra of the suite of 11 excitations that are consistent with the seismic hazard with probability of exceedance 2% in 50 years that were used as input in the numerical analyses.

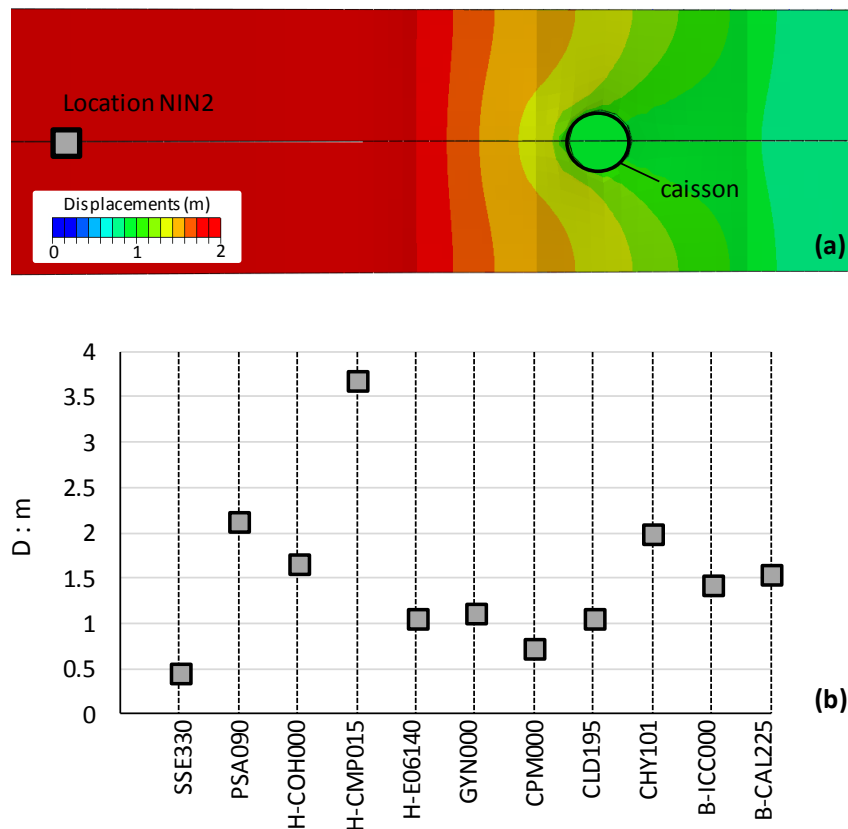


Fig. 8 – Results from analytical step 1: (a) indicative snapshot with superimposed displacement contours and (b) synopsis of residual displacements at location NIN2 (crest).

Fortunately, the caisson–pier system generally moves much less than the slope, as the former partially fulfills its purpose of acting as a retaining structure. An indicative snapshot of the ground surface with residual displacement contours (Fig. 8a) demonstrates that the caisson restrains soil displacements within a limited area in its vicinity causing a 3D mechanism of soil flow. Capturing this mechanism is essential for the realistic prediction of the foundation movements and this is, in fact, the main advantage of employing 3D numerical modelling to study this problem.

Figure 9 summarizes predictions for foundation displacements and pile damage. Results from analytical Step 2 indicate that downslope piles suffer the most owing to the loss of support with the surrounding soil. The deformed model of Fig. 9a indicates the location where maximum curvatures are expected. According to the synopsis graph of Fig. 9b, only two of the considered excitations leave the pile group unscathed (without plastic deformations). By contrast, the majority of the excitations, i.e. six out of 11, result in complete failure of at least six piles (from the 20 of the group) while significant damage should also be expected in the intermediate zone of response ($C_s^{max} > C_s^{yield}$). Such deformations are likely to cause significant distress to the superstructure. The computed permanent foundation displacements shown in Fig. 9b are intended to serve also as input to a detailed structural model aiming to determine the level of structural distress.

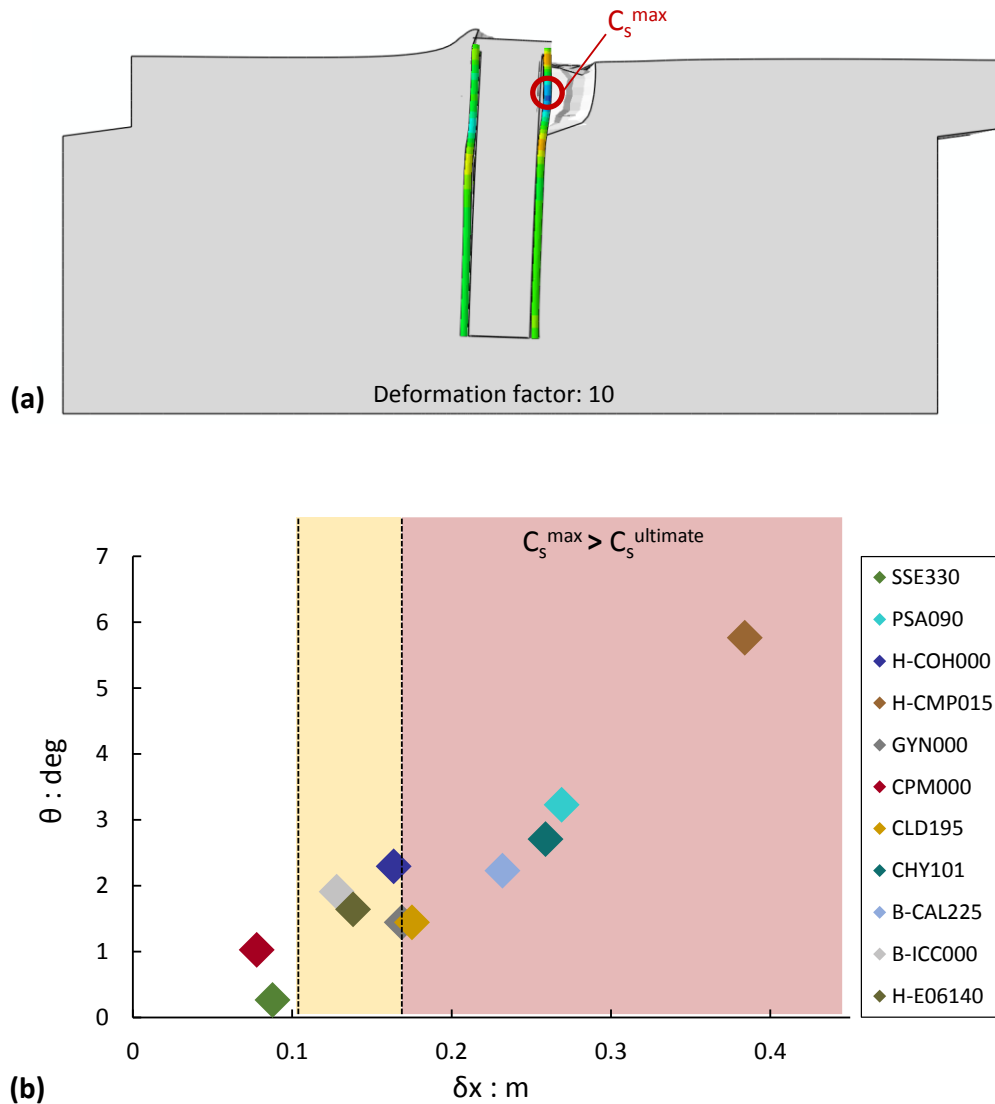


Fig. 9 – Summary of post-earthquake residual deformations of the foundation: (a) deformed ($sf = 10$) snapshot from analytical step 2, and (b) residual displacements with reference to the mid-point of the pile-cap (from Step 1) combined with estimated pile damage (Step 2).

5. Conclusions

The paper has presented a numerical methodology for the analysis of seismic vulnerability of a motorway bridge that interacts with an active landslide. It combines site-specific analysis of the seismic hazard with non-linear 3D numerical modelling of soil–structure interaction and time history analysis. A simplified, hybrid methodology has been adopted to integrate estimation of pile performance with large-scale simulation of the dynamic response of the slope–structure system. Results indicate that a ground motions consistent with an exceedance probability of 2% in 50 years are capable of inflicting substantial permanent pile deformations, and even complete failure, if combined with a fully saturated soil condition (increased water table). Results from this study will be useful for a vulnerability and resilience assessment tool that is under development.



6. Acknowledgements

Financial support has been provided by the Innovation and Networks Executive Agency (INEA) under the powers delegated by the European Commission through the Horizon 2020 program “PANOPTIS–Development of a decision support system for increasing the resilience of transportation infrastructure based on combined use of terrestrial and airborne sensors and advanced modelling tools”, Grant Agreement number 769129. The second author gratefully acknowledges the financial support also provided by the Eugenides Foundation in Greece. Authors are grateful to Panagiotis Panetsos from Egnatia Odos for providing all the necessary data.

7. References

- [1] Monelli D, Pagani M, Weatherill G, Silva V, Crowley H (2012): The hazard component of OpenQuake: The calculation engine of the Global Earthquake Model. *15th World Conference on Earthquake Engineering*, Lisbon, Portugal.
- [2] Giardini D et al. (2013): Seismic Hazard Harmonization in Europe (SHARE): *Online Data Resource*.
- [3] Boore DM, Atkinson GM (2008): Ground-Motion Prediction Equations for the Average Horizontal Component of PGA, PGV, and 5%-Damped PSA at Spectral Periods between 0.01 s and 10.0 s. *Earthquake Spectra*, **24** (1), 99-138.
- [4] Cordova P, Deierlein G, Mehanny SF, Cornell CA (2001): Development of a two-parameter seismic intensity measure and probabilistic assessment procedure. *The Second U.S.-Japan Workshop on Performance-Based Earthquake Engineering Methodology for Reinforced Concrete Building Structures*, Sapporo, Hokkaido, Japan.
- [5] Vamvatsikos D, Cornell CA (2005): Developing efficient scalar and vector intensity measures for IDA capacity estimation by incorporating elastic spectral shape information. *Earthquake Engineering and Structural Dynamics*, **34** (13), 1573-1600.
- [6] Kazantzi AK, Vamvatsikos D (2015): Intensity measure selection for vulnerability studies of building classes. *Earthquake Engineering and Structural Dynamics* **44** (15), 2677-2694.
- [7] Lin T, Haselton CB, Baker JW (2013): Conditional spectrum-based ground motion selection. Part I: Hazard consistency for risk-based assessments. *Earthquake Engineering and Structural Dynamics* **42** (12), 1847-1865.
- [8] Kohrangi M, Bazzurro P, Vamvatsikos D, Spillatura A (2017): Conditional spectrum-based ground motion record selection using average spectral acceleration. *Earthquake Engineering and Structural Dynamics*, **46** (10), 1667-1685.
- [9] Griffiths DV, Lane PA (1999): Slope stability analysis by finite elements. *Géotechnique*, **49** (3), 387-403.
- [10] Kourkoulis R, Gelagoti F, Anastasopoulos I, Gazetas G (2011): Slope Stabilizing Piles and Pile-Groups: Parametric Study and Design Insights. *Journal of Geotechnical and Geoenvironmental Engineering ASCE*, **137** (7), 663-677.
- [11] Anastasopoulos I, Sakellariadis L, Agalinos A (2015): Seismic analysis of motorway bridges accounting for key structural components and non-linear soil – structure interactions. *Soil Dyn. and Earthquake Eng.*, **78**, 127-141.
- [12] Poulos HG (1999): Design of slope stabilizing piles. Slope stability engineering, J. C. Jiang, N. Yagi, and T. Yamagami, eds., Balkema, Rotterdam, Netherlands.
- [13] Anastasopoulos I, Gelagoti F., Kourkoulis R, Gazetas G (2011): Simplified constitutive model for simulation of cyclic response of shallow foundations: validation against laboratory tests. *Journal of Geotechnical and Geoenvironmental Engineering ASCE*, **137** (12), 1154-1168.
- [14] Gerolymos N, Vardoulakis I, Gazetas G (2007): A thermo-poro-visco-plastic shear band model for seismic triggering and evolution of catastrophic landslides. *Soils and Foundations*, **47** (1), 11-25.
- [15] Anastasopoulos I, Gazetas G, Bransby MF, Davies MCR, El Nahas A (2007). Fault rupture propagation through sand: finite element analysis and validation through centrifuge experiments. *Journal of Geotechnical and Geoenvironmental Engineering*, **133** (8), 943-58.